






# Nonmagnetic fractional conductance in high mobility InAs quantum point contacts

I. Villar Rodriguez <sup>1,2,\*</sup>, Y. Gul,<sup>1,2</sup> C. P. Dempsey <sup>3</sup>, J. T. Dong <sup>4</sup>, S. N. Holmes <sup>2</sup>,  
C. J. Palmström,<sup>3,4</sup> and M. Pepper <sup>1,2</sup>

<sup>1</sup>*London Centre for Nanotechnology, University College London, 17-19 Gordon Street, London WC1H 0AH, United Kingdom*

<sup>2</sup>*Department of Electronic and Electrical Engineering, University College London, Torrington Place, London WC1E 7JE, United Kingdom*

<sup>3</sup>*Department of Electrical and Computer Engineering, University of California, Santa Barbara, California 93106, USA*

<sup>4</sup>*Materials Department, University of California, Santa Barbara, California 93106, USA*



(Received 28 February 2025; revised 24 June 2025; accepted 8 July 2025; published 4 August 2025)

In this paper, we report the magnetoelectronic properties of high mobility InAs quantum point contacts grown on InP substrates. The InAs quantum well is embedded between  $\text{In}_{0.72}\text{Ga}_{0.28}\text{As}$  cladding layers and  $\text{In}_{0.81}\text{Al}_{0.19}\text{As}$  barrier layers, and is populated via self-accumulation. The one-dimensional (1D) conductance reaches a maximum value of 17 plateaus, quantized in units of  $2e^2/h$ , where  $e$  is the fundamental unit of charge and  $h$  is Planck's constant. The in-plane effective  $g$  factor was estimated to be  $-10.9 \pm 1.5$  for subband  $N = 1$  and  $-10.8 \pm 1.6$  for subband  $N = 2$ . Furthermore, a study of the nonmagnetic fractional conductance states at  $0.2 (e^2/h)$  and  $0.1 (e^2/h)$  is provided. While their origin remains under discussion, evidence suggests that they arise from strong electron-electron interactions and momentum-conserving backscattering between electrons in two distinct channels within the 1D region. This phenomenon may also be interpreted as an entanglement between the two channel directions facilitated by momentum-conserving backscattering.

DOI: [10.1103/45nh-cld6](https://doi.org/10.1103/45nh-cld6)

## I. INTRODUCTION

Quantization of conductance in units of  $2e^2/h$  in one-dimensional (1D) quantum point contacts (QPCs) was first observed by Wharam [1] and van Wees [2] when investigating a gate-controlled channel defined in the two-dimensional electron gas (2DEG) of a GaAs/AlGaAs heterostructure. Since then, many reports have studied the interesting physics of these constrictions: the effect of a source-drain bias voltage [3,4], the appearance of the 0.7 conductance anomaly [5–9], and many-body effects [10–13]. One of the most highlighted recent advances in the field demonstrated the potential to spatially manipulate electron spins in a QPC [14–16]. This is a crucial component for spin-based technologies. Additionally, the realization of an all-electrical spin field-effect transistor was achieved through the implementation of two QPCs [17].

The 1D quantization of conductance is observed in ballistic constrictions where the mean free path of the electrons is larger than the size of the split gates. Therefore, high quality heterostructures with high 2DEG electron mobility are required. Furthermore, a 2DEG with strong spin-orbit coupling (SOC) would facilitate the manipulation of the electron spins. A material that meets all these requirements would be an ideal candidate for spintronic and quantum information devices.

High electron mobility InAs quantum wells (QWs) have been grown in both lattice-matched GaSb [18,19] and lattice-mismatched InP [20,21] substrates. However, the reported presence of sidewall conduction in InAs QWs grown on GaSb substrates [22] makes InP a better choice. Moreover, recent advancements [23] in wafer manufacturing have improved upon the current state-of-the-art QW thickness  $t_{\text{QW}}$  ( $t_{\text{QW}} = 4$  nm for  $\text{In}_{0.75}\text{Al}_{0.25}\text{As}$  [21] barrier layers and  $t_{\text{QW}} = 7$  nm for  $\text{In}_{0.81}\text{Al}_{0.19}\text{As}$  [24] barrier layers) of InAs QWs grown on InP substrates. This advancement shows an improvement in the highest achievable mobility. Other significant properties of InAs include its small effective mass [25] and its large bulk  $g$  factor. For comparison, the  $g$  factor of bulk InAs is  $-15$  [26], which is considerably larger than that of InGaAs ( $-9$ ) [27] or GaAs ( $-0.44$ ) [28]. Furthermore, InAs exhibits strong SOC that allows efficient control of spin currents. The large  $g$  factor of InAs leads to Zeeman splitting at low magnetic fields, which in proximity to an  $s$ -wave superconductor could introduce Majorana zero modes [29–32] that can be utilized for topological quantum computing applications [33]. Several studies have already been conducted on 1D InAs QPCs [20,34–36], with a maximum of eight pronounced quantized conductance plateaus observed at 1.5 K [37].

Strong electron-electron interactions occur when the carrier density in the QPC is low. In this state, nonmagnetic fractional quantization of conductance has previously been reported in strained-Ge [38], InGaAs [39], and GaAs [40] QWs. Although the origin of these new quantum states is not fully understood, their study could lead to future applications in quantum computing.

In this work, we present the magnetotransport properties of gate-defined 1D QPCs fabricated on InAs QWs grown on

\*Contact author: [uceeivi@ucl.ac.uk](mailto:uceeivi@ucl.ac.uk)

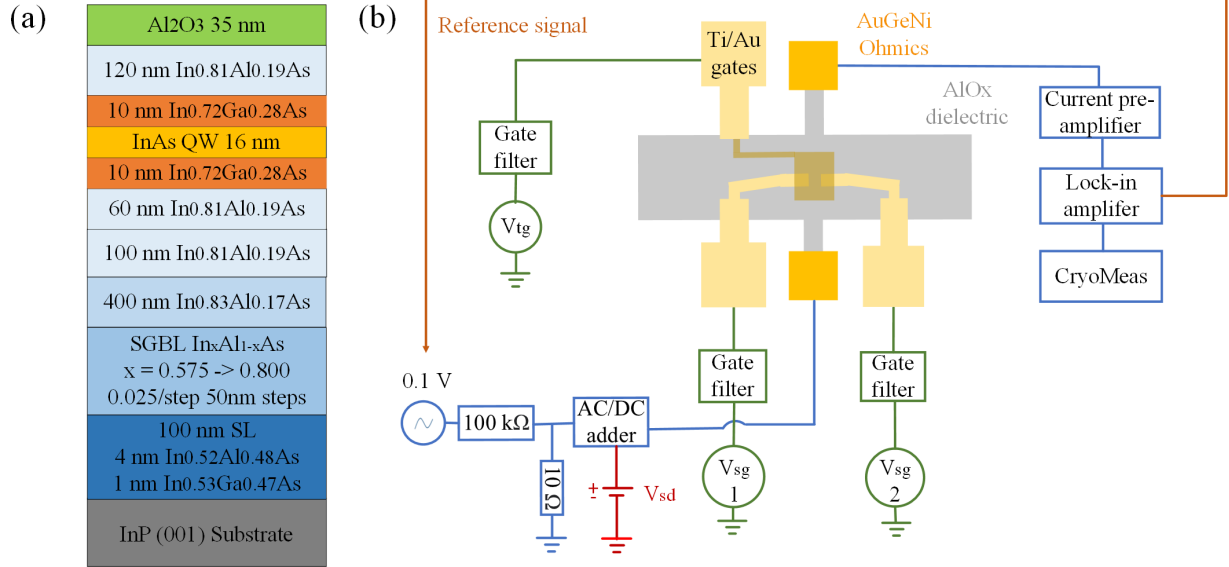


FIG. 1. (a) Schematic of the wafer structure with the added dielectric layer. (b) Two-terminal conductance measurement setup. A constant ac differential voltage drop across the device is applied using a potential divider. A dc source-drain bias voltage,  $V_{sd}$ , can be superimposed onto the signal using an ac/dc adder. All gates are protected by a low pass gate filter. The outgoing signal is amplified by a current preamplifier and measured by a lock-in amplifier. CRYOMEAS [41] is the program utilized to record the data.

InP substrates, with QW thicknesses exceeding those reported in earlier studies. We demonstrate clean and controllable 1D behavior. Furthermore, strong electron-electron interactions at low carrier densities are investigated. Here, nonmagnetic fractional quantization of conductance is observed, and possible effects leading to this phenomenon are discussed.

## II. DEVICE FABRICATION AND EXPERIMENTAL SETUP

The device presented in this work is an InAs QW heterostructure grown on a semi-insulating Fe-doped InP (001) substrate by molecular beam epitaxy. The 2DEG lies 130 nm below the surface and is surrounded by  $\text{In}_{0.72}\text{Ga}_{0.28}\text{As}$  cladding layers and  $\text{In}_{0.81}\text{Al}_{0.19}\text{As}$  barrier layers. The heterostructure is nominally undoped; however, the 2DEG forms via self-accumulation [42,43], with carriers likely originating from donors in the  $\text{In}_{0.81}\text{Al}_{0.19}\text{As}$  barrier layers. The width of the QW is 16 nm, exceeding the maximum previously achievable width for InAs QWs grown on InP substrates [21,24]. A diagram of the wafer structure is shown in Fig. 1(a). A more detailed explanation of the growth conditions can be found in Ref. [23].

For 1D electrical and magnetotransport measurements, Hall bars of 1400  $\mu\text{m}$  in length and 80  $\mu\text{m}$  in width were fabricated. Using a mixture of  $\text{H}_2\text{SO}_4:\text{H}_2\text{O}_2:\text{H}_2\text{O}$  (1:8:120), the Hall bar mesa was etched so that the QPC channel lies along the  $[1\bar{1}0]$  direction. This orientation was chosen because the electron mobility is largest in this direction [44]. AuGeNi Ohmic contacts connecting the 2DEG and the surface were evaporated onto the sample and annealed at 450  $^\circ\text{C}$  for 2 min. To insulate the 2DEG from the gates, a 35-nm  $\text{Al}_2\text{O}_3$  dielectric layer was deposited using atomic layer deposition after cleaning the surface with buffered hydrofluoric acid. Windows for the Ohmic contacts were opened by etching through the dielectric. Finally, the split gates and QPC top gates were

patterned onto the wafer using electron beam lithography. Cross-linked polymethyl methacrylate was used as a dielectric between the split gates and the QPC top gates, and Ti/Au was deposited to form the gates. The results presented in this paper were obtained from split gates measuring 500 nm in length and width or 400 nm in length and 500 nm in width. At 1.5 K, the 2DEG carrier density is  $3.6 \times 10^{11} \text{ cm}^{-2}$ , and the electron mobility is  $9.3 \times 10^5 \text{ cm}^2 \text{ V s}$ . The effective electron mass and the Rashba coefficient were determined as  $(0.031 \pm 0.002)m_e$ , where  $m_e$  is the rest electron mass, and  $12 \times 10^{-12} \text{ eV m}$ , respectively [23]. All of these parameters were extracted at zero Hall bar top gate voltage.

In all experiments, the two-terminal differential conductance ( $G$ ) was measured as a function of split gate voltage ( $V_{sg}$ ), while a 10  $\mu\text{V}$  ac voltage at 33 Hz was applied. The experiments in Secs. III A and III B were performed with the QPC top gate voltage  $V_{tg} = 0 \text{ V}$ , whereas in Sec. III C,  $V_{tg}$  was held constant at a negative value during each split gate sweep. The split gates were biased symmetrically unless stated otherwise. The measurements were taken without illumination in a cryo-free dilution refrigerator at 220 mK over multiple cooldowns. The gates were grounded during cooldown. The measurement configuration is shown in Fig. 1(b).

## III. RESULTS AND DISCUSSION

### A. 1D conductance quantization

Figure 2 illustrates the quantized 1D conductance as the split gate voltage is raised from the pinch-off state. We observe 17 plateaus quantized in units of  $2e^2/h$ , which is twice the number reported in earlier studies [20,34–37]. This finding underscores the high material quality and indicates ballistic transport in the gate-defined 1D QPCs. The observed conductance trace is consistent across different cooldown cycles, but it shows a gradual shift toward more negative

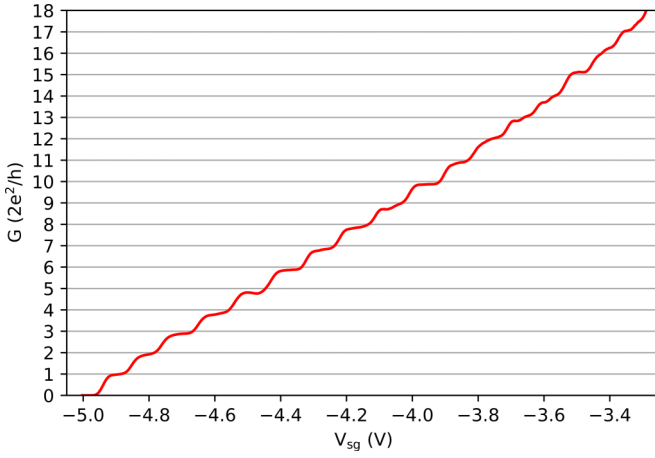


FIG. 2.  $G$  as a function of  $V_{sg}$  when  $V_{lg} = 0$  V. The split gate dimensions are 400 nm in length and 500 nm in width, and up to 17 plateaus quantized in units of  $2e^2/h$  can be observed. The series resistance for this measurement was 1.3 k $\Omega$ , determined individually at each cooldown and each QPC.

pinch-off voltages with repeated voltage sweeps. This drift can be attributed to interactions between large applied split gate voltages and charge traps within the dielectric layer [37,45]. To mitigate this, we employed slightly larger split gates (500 nm in width and length), resulting in a more stable pinch-off voltage and minimal drift, suggesting dielectric charging as a primary cause of the shift.

### B. Calculation of the in-plane effective $g$ factor

The effective  $g$  factor,  $g^*$ , was estimated by analyzing the Zeeman splitting under an applied in-plane magnetic field,  $B$ , and the subband spacing by applying a dc source-drain bias voltage,  $V_{sd}$ , using the expression [46]

$$|g^*| = \frac{1}{\mu_B} \frac{d(\Delta E_z)}{dB} = \frac{e}{\mu_B} \frac{\delta V_{sd}}{\delta V_{sg}} \frac{\delta V_{sg}}{\delta B}, \quad (1)$$

where  $\mu_B$  is the Bohr magneton and  $E_z$  represents the Zeeman energy.

Clear Zeeman spin splitting is observed when applying an in-plane magnetic field, as shown in Fig. 3. The splitting is visible at approximately 2 T. As the magnetic field increases, odd-numbered plateaus emerge while the even-numbered disappear. At sufficiently high magnetic fields, crossing of the spin-split subbands is observed before the reappearance of the even-numbered plateaus. This crossover point allows the extraction of  $\delta V_{sg}$ , which, when divided by the corresponding magnetic field, yields  $\delta V_{sg}/\delta B$ .

Figure 4(a) depicts 1D conductance traces under varying dc bias voltages. When a high dc bias is applied, the momentum degeneracy is lifted [47] and the spin-degenerate plateaus evolve into  $0.5 (2e^2/h)$ ,  $1.5 (2e^2/h)$ ,  $2.5 (2e^2/h)$ , etc. For negative dc bias, this behavior is apparent, however, for positive dc bias, a distinct plateau at  $0.25 (2e^2/h)$  can be seen. This effect has been observed before in InGaAs [46] and GaAs [47] heterostructures, where the asymmetric behavior was attributed to the formation of a density wave or skyrmion [46]. In the case of GaAs [47], the emergence of the  $0.25$

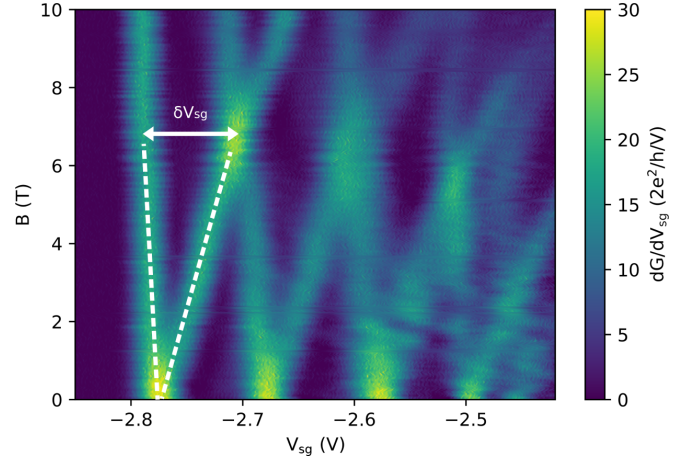


FIG. 3. Transconductance ( $dG/dV_{sg}$ ) plotted as a function of in-plane  $B$  on the  $y$  axis and  $V_{sg}$  on the  $x$  axis. The bright yellow lines correspond to rises in conductance, while the blue dark regions signify the quantized plateaus. Subband crossings are also visible.

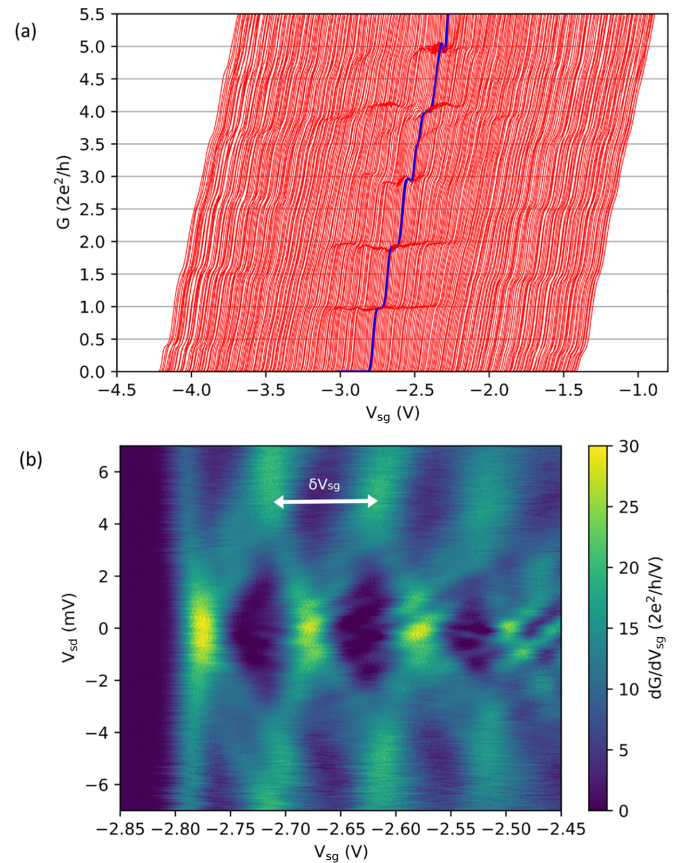


FIG. 4. (a)  $G$  as a function of  $V_{sg}$  for different values of  $V_{sd}$  varying from  $-7$  mV (left) to  $7$  mV (right) in  $0.05$  mV steps. The blue trace corresponds to  $V_{sd} = 0$  V. For display purposes, the traces have been shifted laterally by  $10$  mV. The series resistance for this measurement was  $1.6$  k $\Omega$ . (b) Transconductance ( $dG/dV_{sg}$ ) plotted as a function of  $V_{sd}$  on the  $y$  axis and  $V_{sg}$  on the  $x$  axis. The blue dark regions correspond to the quantized plateaus, while the brighter yellow regions indicate the subband transitions where  $dG/dV_{sg}$  is large.



TABLE I. Extracted parameters for the Zeeman splitting and subband spacing crossings used to determine  $g^*$ .

Subband	$N = 1$	$N = 2$
$\delta V_{sg}/\delta B$ ( $10^{-2}$ V/T)	$1.21 \pm 0.06$	$1.43 \pm 0.11$
$\delta V_{sd}/\delta V_{sg}$ (mV/V)	$52.2 \pm 6.6$	$43.8 \pm 5.5$
$g^*$	$-10.9 \pm 1.5$	$-10.8 \pm 1.6$

( $2e^2/h$ ) structure was linked to the creation of a unidirectional spin-polarized current. The transconductance as a function of  $V_{sd}$  and  $V_{sg}$  in Fig. 4(b) shows how the even diamonds evolve into odd-quantized values. The intersection where two subbands cross can be used to extract  $\delta V_{sd}/\delta V_{sg}$ .

The effective  $g$  factor for each subband  $N$  was then determined using Eq. (1). The variables necessary for this calculation are provided in Table I. The computed effective  $g$  factor is of similar order to that reported in previous studies on InAs QWs [37].

### C. Nonmagnetic fractional conductance quantization

The observation of nonmagnetic fractional quantization of conductance typically occurs at low carrier densities and asymmetric confining potentials [38–40]. To investigate fractional conductance quantization in the 1D InAs QPCs, the carrier density was reduced by applying a negative voltage to the QPC top gate. As the QPC top gate voltage became increasingly negative, a sudden transition in conductance was observed in the ground state, shifting from  $2e^2/h$  to  $2$  ( $2e^2/h$ ), as indicated in Fig. 5. This transition preceded the emergence of fractional conductance plateaus and may suggest the formation of a zigzag incipient Wigner crystal [12].

The 0.2 and 0.1 ( $e^2/h$ ) fractions, previously observed in InGaAs [39], are seen in InAs at low carrier densities. Both fractional states persist even as the temperature increases, as shown in Fig. 6. Combined with multiple cooldown measurements, this suggests that these nonmagnetic fractional states are not caused by disorder. The slight lifting of the plateaus

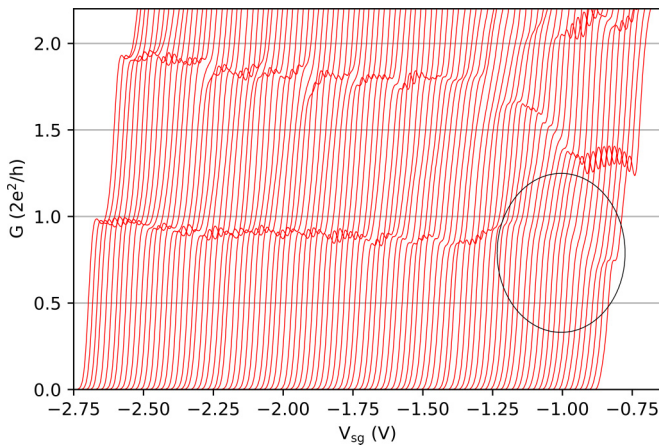


FIG. 5.  $G$  as a function of  $V_{sg}$  for different values of  $V_{tg}$ , ranging from 0 V (left) to  $-2$  V (right). The encircled region highlights the suppression of the  $2e^2/h$  conductance plateau, which occurs around  $V_{tg} = -1.7$  V.

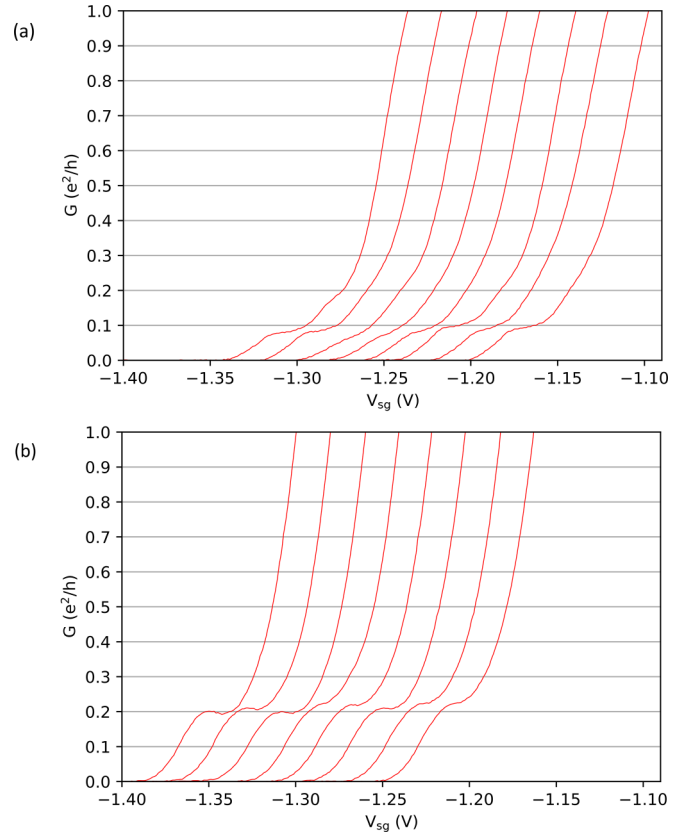


FIG. 6. Temperature dependence of the (a) 0.1 ( $e^2/h$ ) and (b) 0.2 ( $e^2/h$ ) plateaus. The 0.1 ( $e^2/h$ ) plateau was observed at  $V_{tg} = -3.03$  V, while the 0.2 ( $e^2/h$ ) plateau was observed at  $V_{tg} = -2.93$  V. The temperature was varied from 220 mK (left) up to 920 mK (right) in 100 mK steps. For clarity, the traces have been shifted horizontally by 20 mV.

from their quantized value with temperature is consistent with predictions by Shavit and Oreg [48]. Their theoretical model allows for nonmagnetic fractional conductance quantization through momentum-conserving backscattering of electrons in two distinct spin subbands or transverse channels, such as those formed in a zigzag incipient Wigner crystal. As a result, the two zigzag channels may become entangled. The resulting conductance is given by

$$G = \frac{(n_1 - n_2)^2}{n_1^2 + n_2^2} \left( \frac{e^2}{h} \right), \quad (2)$$

where  $n_1, n_2$  represent the number of backscattered electrons from subbands 1,2. This model predicts the 0.2 ( $e^2/h$ ) plateau when  $n_1 = 1, 2$  and  $n_2 = 2, 4$ , but it does not explain the formation of the 0.1 ( $e^2/h$ ) plateau. A scenario where channel 1 is decoupled from the leads but confined within the wire and strongly interacts with the other channel could yield a conductance of  $G = n_1^2/(n_1^2 + n_2^2)$  [48], potentially explaining the 0.1 ( $e^2/h$ ) state for  $n_1 = 1$  and  $n_2 = 3$ . However, no evidence of channel 1 being confined within the wire is observed in this study. Further investigations are necessary to elucidate the origin of the 0.1 ( $e^2/h$ ) plateau.

Between the two QPC top gate voltages where the fractional plateaus appear, the 0.2 ( $e^2/h$ ) plateau evolves into the

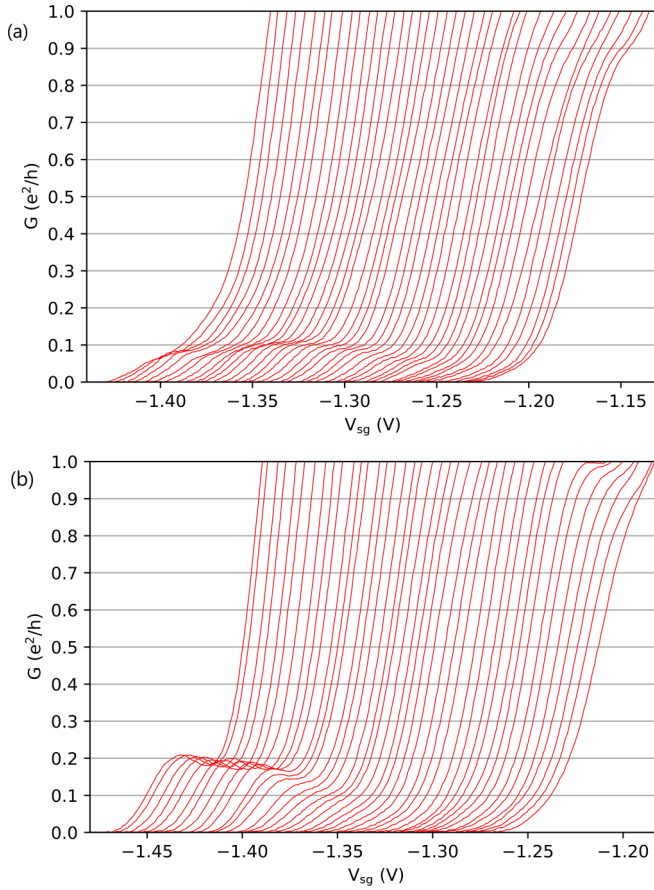


FIG. 7.  $G$  as a function of  $V_{sg}$  under an in-plane magnetic field perpendicular to the current direction, varying from 0 T (left) to 2 T (right), for the (a)  $0.1 (e^2/h)$  and (b)  $0.2 (e^2/h)$  plateaus. The  $0.2 (e^2/h)$  plateau vanishes at a lower magnetic field than the  $0.1 (e^2/h)$  plateau.

$0.1 (e^2/h)$  plateau. This behavior remains consistent with the theory of Shavit and Oreg, as reducing the QPC top gate voltage, and thus the carrier concentration, alters the number of available scattering states between the two channels, allowing one fractional state to evolve into the other.

Applying a magnetic field to these fractional states reveals deviations from previous observations in InGaAs systems [39]. In InGaAs, the fractions persisted under the application of an in-plane magnetic field parallel to the current direction but disappeared when the field was applied in plane and perpendicular to the current. In contrast, in InAs, the fractions vanish under an in-plane magnetic field regardless of its orientation relative to the current, as shown in Fig. 7.

In InGaAs systems, the formation of fractional conductance states has been attributed to electron backscattering between Rashba spin-split subbands, separated in  $k$  space. When the magnetic field was parallel to the current, a spin gap formed, enabling backscattering between the spin-split subbands. Conversely, when the magnetic field was perpendicular, one of the spin-split subbands shifted up in energy, preventing backscattering and thereby causing the fractions to disappear. However, the distinct behavior observed in our InAs devices suggests that our states are not spin polarized and do not arise from momentum-conserving backscatter-

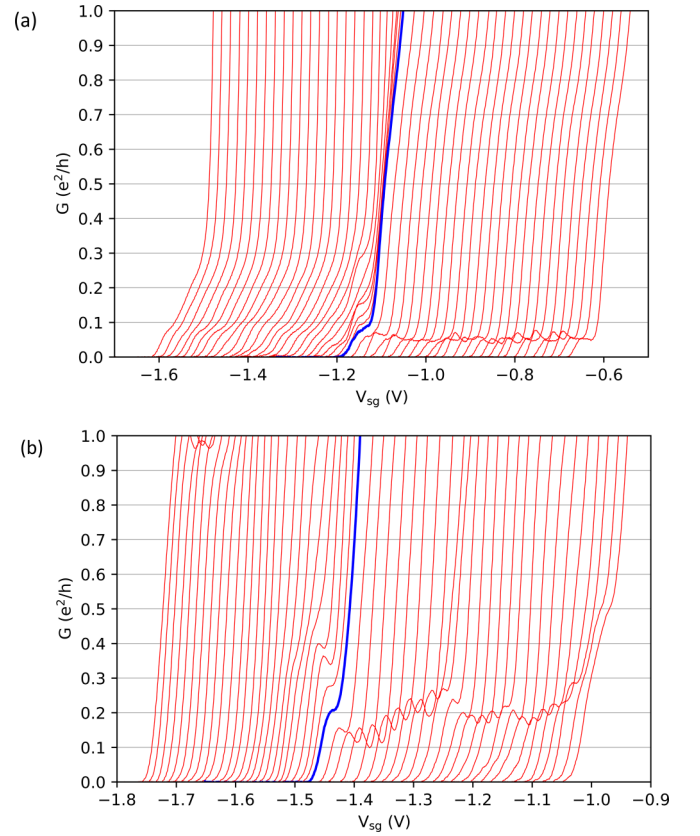


FIG. 8.  $G$  as a function of  $V_{sg}$  with varying degrees of lateral asymmetric confinement, reaching a maximum shift of  $\Delta V_{sg} = \pm 0.5$  V on each side of the graph, for the (a)  $0.1 (e^2/h)$  and (b)  $0.2 (e^2/h)$  plateaus. The blue trace corresponds to symmetrically biased split gates.

ing between electrons in different spin subbands. Instead, it raises the possibility that they result from backscattering between different transverse channels within a Wigner crystal, where the dispersion bands align in  $k$  space. In this scenario, the application of a magnetic field in any direction shifts one of the subbands to higher energy, thereby suppressing the backscattering process.

This difference can be explained by examining the wafer structures. The InGaAs wafers are intentionally Si doped, which enhances the Rashba asymmetry across the QW. In contrast, the InAs wafers are nominally undoped. Additionally, the InGaAs QWs are in direct contact with the InAlAs barriers, whereas in the InAs structures, the electron wave function exhibits minimal penetration into the InAlAs layer [49]. The combination of reduced doping and limited wavefunction overlap with the barrier material results in a lower structural asymmetry in the InAs QWs, thereby suppressing Rashba spin splitting and accounting for the observed differences in behavior.

Figure 8 shows the conductance measured under varying lateral asymmetric potentials,  $\Delta V_{sg}$ , which displace the entire ballistic channel in real space, exposing it to a different electrostatic environment. Fractional plateau formation is preserved for one polarity of asymmetry but suppressed for the opposite. Under negative asymmetry, the  $0.2 (e^2/h)$  plateau

disappears entirely, while the  $0.1 (e^2/h)$  plateau weakens, initially increasing in value and subsequently oscillating around its nominal value. In contrast, under positive asymmetry, the  $0.1 (e^2/h)$  plateau is halved in value, and the  $0.2 (e^2/h)$  plateau exhibits oscillations around its nominal position. This asymmetry-dependent behavior, where one polarity preserves the fractional plateaus while the other suppresses them, has been consistently observed across two separate cooldowns. Further experiments are needed to conclusively identify the origin of this behavior.

An interesting aspect of these fractional electron states is their potential to demonstrate fractional charge. Numerous studies [50–54] have investigated fractional charge in fractional quantum Hall effect (FQHE) systems through shot noise experiments. The detection of fractional charge in these InAs fractional conductance states could provide new opportunities to investigate whether they exhibit non-Abelian properties, potentially playing a crucial role in the development of topological quantum computing. To enable such investigations, high reproducibility of the fractional states is essential.

#### IV. CONCLUSION

In summary, we have demonstrated high mobility ballistic transport in 1D InAs QPCs, with conductance quantization observed up to  $17 (2e^2/h)$ . The in-plane effective  $g$  factor was calculated to be  $-10.9 \pm 1.5$  for  $N = 1$  and  $-10.8 \pm 1.6$  for  $N = 2$ , determined from the intersection of spin-split and momentum-split subbands.

Additionally, we have provided evidence for nonmagnetic fractional quantization of conductance. Our experiments demonstrate that these states persist at elevated temperatures, are not spin polarized, and their occurrence is preserved under one direction of lateral asymmetric bias while being suppressed in the opposite direction. This provides experimental

support for the theoretical model presented in Ref. [48], which suggests that nonmagnetic fractional conductance quantization can arise from strong electron-electron interactions and momentum-conserving backscattering between electrons in distinct subbands.

The data further suggest the potential formation of a zigzag incipient Wigner crystal, where backscattering between the two transverse channels could result in fraction formation and entanglement. Further investigation is required to elucidate the origin of these fractions and their associated subband configurations.

The unique properties of InAs combined with these fractional states suggest promising future applications in spintronic devices and quantum computing systems.

#### ACKNOWLEDGMENTS

The authors acknowledge financial support from the U.S. Department of Energy under Award No. DE-SC0019274 for the MBE growth and sample characterization at UCSB (C.P.D., J.T.D., C.J.P.), the UK Science and Technology Facilities Council (Award No. ST/Y005074/1), and the Engineering and Physical Sciences Research Council (Grants No. EP/R029075/1 and No. EP/N509577/1) for the quantum point contact device fabrication and cryogenic transport measurement (I.V.R., Y.G., S.N.H., M.P.). We are also grateful for the use of the shared facilities of the NSF Materials Research Science and Engineering Center at UCSB (Grant No. DMR 2308708), the UCSB Nanofabrication Facility, and the SP Cleanroom at the University of Cambridge for access to their fabrication facilities.

#### DATA AVAILABILITY

The data that support the findings of this article are not publicly available. The data are available from the authors upon reasonable request.

- 
- [1] D. A. Wharam, T. J. Thornton, R. Newbury, M. Pepper, H. Ahmed, J. E. F. Frost, D. G. Hasko, D. C. Peacock, D. A. Ritchie, and G. A. C. Jones, One-dimensional transport and the quantisation of the ballistic resistance, *J. Phys. C: Solid State Phys.* **21**, L209 (1988).
  - [2] B. J. van Wees, H. van Houten, C. W. J. Beenakker, J. G. Williamson, L. P. Kouwenhoven, D. van der Marel, and C. T. Foxon, Quantized conductance of point contacts in a two-dimensional electron gas, *Phys. Rev. Lett.* **60**, 848 (1988).
  - [3] N. K. Patel, J. T. Nicholls, L. Martin-Moreno, M. Pepper, J. E. F. Frost, D. A. Ritchie, and G. A. C. Jones, Evolution of half plateaus as a function of electric field in a ballistic quasi-one-dimensional constriction, *Phys. Rev. B* **44**, 13549 (1991).
  - [4] L. P. Kouwenhoven, B. J. van Wees, C. J. P. M. Harmans, J. G. Williamson, H. van Houten, C. W. J. Beenakker, C. T. Foxon, and J. J. Harris, Nonlinear conductance of quantum point contacts, *Phys. Rev. B* **39**, 8040 (1989).
  - [5] K. J. Thomas, J. T. Nicholls, M. Y. Simmons, M. Pepper, D. R. Mace, and D. A. Ritchie, Possible spin polarization in a one-dimensional electron gas, *Phys. Rev. Lett.* **77**, 135 (1996).
  - [6] A. Kristensen, H. Bruus, A. E. Hansen, J. B. Jensen, P. E. Lindelof, C. J. Marckmann, J. Nygård, C. B. Sørensen, F. Beuscher, A. Forchel, and M. Michel, Bias and temperature dependence of the 0.7 conductance anomaly in quantum point contacts, *Phys. Rev. B* **62**, 10950 (2000).
  - [7] S. M. Cronenwett, H. J. Lynch, D. Goldhaber-Gordon, L. P. Kouwenhoven, C. M. Marcus, K. Hirose, N. S. Wingreen, and V. Umansky, Low-temperature fate of the 0.7 structure in a point contact: A Kondo-like correlated state in an open system, *Phys. Rev. Lett.* **88**, 226805 (2002).
  - [8] M. J. Iqbal, R. Levy, E. J. Koop, J. B. Dekker, J. P. de Jong, J. H. M. van der Velde, D. Reuter, A. D. Wieck, R. Aguado, Y. Meir, and C. H. van der Wal, Odd and even Kondo effects from emergent localization in quantum point contacts, *Nature (London)* **501**, 79 (2013).
  - [9] F. Bauer, J. Heyder, E. Schubert, D. Borowsky, D. Taubert, B. Bruognolo, D. Schuh, W. Wegscheider, J. von Delft, and S. Ludwig, Microscopic origin of the ‘0.7-anomaly’ in quantum point contacts, *Nature (London)* **501**, 73 (2013).



- [10] W. K. Hew, K. J. Thomas, M. Pepper, I. Farrer, D. Anderson, G. A. C. Jones, and D. A. Ritchie, Incipient formation of an electron lattice in a weakly confined quantum wire, *Phys. Rev. Lett.* **102**, 056804 (2009).
- [11] L. W. Smith, W. K. Hew, K. J. Thomas, M. Pepper, I. Farrer, D. Anderson, G. A. C. Jones, and D. A. Ritchie, Row coupling in an interacting quasi-one-dimensional quantum wire investigated using transport measurements, *Phys. Rev. B* **80**, 041306(R) (2009).
- [12] S. Kumar, K. J. Thomas, L. W. Smith, M. Pepper, G. L. Creeth, I. Farrer, D. Ritchie, G. Jones, and J. Griffiths, Many-body effects in a quasi-one-dimensional electron gas, *Phys. Rev. B* **90**, 201304(R) (2014).
- [13] J. S. Meyer and K. A. Matveev, Wigner crystal physics in quantum wires, *J. Phys.: Condens. Matter* **21**, 023203 (2009).
- [14] S.-T. Lo, C.-H. Chen, J.-C. Fan, L. W. Smith, G. L. Creeth, C.-W. Chang, M. Pepper, J. P. Griffiths, I. Farrer, H. E. Beere, G. A. C. Jones, D. A. Ritchie, and T.-M. Chen, Controlled spatial separation of spins and coherent dynamics in spin-orbit-coupled nanostructures, *Nat. Commun.* **8**, 15997 (2017).
- [15] T.-M. Chen, M. Pepper, I. Farrer, G. A. C. Jones, and D. A. Ritchie, All-electrical injection and detection of a spin-polarized current using 1D conductors, *Phys. Rev. Lett.* **109**, 177202 (2012).
- [16] P. Debray, S. M. S. Rahman, R. S. N. J. Wan, M. Cahay, A. T. Ngo, S. E. Ulloa, S. T. Herbert, M. Muhammad, and M. Johnson, All-electric quantum point contact spin-polarizer, *Nat. Nanotechnol.* **4**, 759 (2009).
- [17] P. Chuang, S.-C. Ho, L. W. Smith, F. Sfigakis, M. Pepper, C.-H. Chen, J.-C. Fan, J. P. Griffiths, I. Farrer, H. E. Beere, G. A. C. Jones, D. A. Ritchie, and T.-M. Chen, All-electric all-semiconductor spin field-effect transistors, *Nat. Nanotechnol.* **10**, 35 (2015).
- [18] T. Tschirky, S. Mueller, C. A. Lehner, S. Fält, T. Ihn, K. Ensslin, and W. Wegscheider, Scattering mechanisms of highest-mobility InAs/Al<sub>x</sub>Ga<sub>1-x</sub>Sb quantum wells, *Phys. Rev. B* **95**, 115304 (2017).
- [19] C. Thomas, A. T. Hatke, A. Tuaz, R. Kallagher, T. Wu, T. Wang, R. E. Diaz, G. C. Gardner, M. A. Capano, and M. J. Manfra, High-mobility InAs 2DEGs on GaSb substrates: A platform for mesoscopic quantum transport, *Phys. Rev. Mater.* **2**, 104602 (2018).
- [20] J. Shabani, A. P. McFadden, B. Shojaei, and C. J. Palmstrøm, Gating of high-mobility InAs metamorphic heterostructures, *Appl. Phys. Lett.* **105**, 262105 (2014).
- [21] A. T. Hatke, T. Wang, C. Thomas, G. C. Gardner, and M. J. Manfra, Mobility in excess of  $10^6$  cm<sup>2</sup>/V s in InAs quantum wells grown on lattice mismatched InP substrates, *Appl. Phys. Lett.* **111**, 142106 (2017).
- [22] S. Mueller, C. Mittag, T. Tschirky, C. Charpentier, W. Wegscheider, K. Ensslin, and T. Ihn, Edge transport in InAs and InAs/GaSb quantum wells, *Phys. Rev. B* **96**, 075406 (2017).
- [23] C. P. Dempsey, J. T. Dong, I. Villar Rodriguez, Y. Gul, S. Chatterjee, M. Pendharkar, S. N. Holmes, M. Pepper, and C. J. Palmstrøm, Effects of strain compensation on electron mobilities in InAs quantum wells grown on InP(001), *Phys. Rev. Mater.* **9**, 054607 (2025).
- [24] A. Benali, P. Rajak, R. Ciano, J. Plaisier, S. Heun, and G. Biasiol, Metamorphic InAs/InGaAs QWs with electron mobilities exceeding  $7 \times 10^5$  cm<sup>2</sup>/V s, *J. Cryst. Growth* **593**, 126768 (2022).
- [25] J. Shabani, S. Das Sarma, and C. J. Palmstrøm, An apparent metal-insulator transition in high-mobility two-dimensional InAs heterostructures, *Phys. Rev. B* **90**, 161303(R) (2014).
- [26] C. R. Pidgeon, D. L. Mitchell, and R. N. Brown, Interband magnetoabsorption in InAs and InSb, *Phys. Rev.* **154**, 737 (1967).
- [27] W. Desrat, F. Giazotto, V. Pellegrini, F. Beltram, F. Capotondi, G. Biasiol, L. Sorba, and D. K. Maude, Magnetotransport in high-g-factor low-density two-dimensional electron systems confined in In<sub>0.75</sub>Ga<sub>0.25</sub>As/In<sub>0.75</sub>Al<sub>0.25</sub>As quantum wells, *Phys. Rev. B* **69**, 245324 (2004).
- [28] M. J. Snelling, G. P. Flinn, A. S. Plaut, R. T. Harley, A. C. Tropper, R. Eccleston, and C. C. Phillips, Magnetic *g* factor of electrons in GaAs/Al<sub>x</sub>Ga<sub>1-x</sub>As quantum wells, *Phys. Rev. B* **44**, 11345 (1991).
- [29] A. Das, Y. Ronen, Y. Most, Y. Oreg, M. Heiblum, and H. Shtrikman, Zero-bias peaks and splitting in an Al-InAs nanowire topological superconductor as a signature of Majorana fermions, *Nat. Phys.* **8**, 887 (2012).
- [30] R. M. Lutchyn, J. D. Sau, and S. Das Sarma, Majorana fermions and a topological phase transition in semiconductor-superconductor heterostructures, *Phys. Rev. Lett.* **105**, 077001 (2010).
- [31] Y. Oreg, G. Refael, and F. von Oppen, Helical liquids and Majorana bound states in quantum wires, *Phys. Rev. Lett.* **105**, 177002 (2010).
- [32] Microsoft Azure Quantum, Interferometric single-shot parity measurement in InAs-Al hybrid devices, *Nature (London)* **638**, 651 (2025).
- [33] S. Sarma, M. Freedman, and C. Nayak, Majorana zero modes and topological quantum computation, *npj Quantum Inf.* **1**, 15001 (2015).
- [34] S. Matsuo, H. Kamata, S. Baba, R. S. Deacon, J. Shabani, C. J. Palmstrøm, and S. Tarucha, Magnetic field inducing Zeeman splitting and anomalous conductance reduction of half-integer quantized plateaus in InAs quantum wires, *Phys. Rev. B* **96**, 201404(R) (2017).
- [35] C. Mittag, M. Karalic, Z. Lei, C. Thomas, A. Tuaz, A. T. Hatke, G. C. Gardner, M. J. Manfra, T. Ihn, and K. Ensslin, Gate-defined quantum point contact in an InAs two-dimensional electron gas, *Phys. Rev. B* **100**, 075422 (2019).
- [36] J. S. Lee, B. Shojaei, M. Pendharkar, A. P. McFadden, Y. Kim, H. J. Suominen, M. Kjaergaard, F. Nichele, H. Zhang, C. M. Marcus, and C. J. Palmstrøm, Transport studies of epi-Al/InAs two-dimensional electron gas systems for required building-blocks in topological superconductor networks, *Nano Lett.* **19**, 3083 (2019).
- [37] C. L. Hsueh, P. Sriram, T. Wang, C. Thomas, G. Gardner, M. A. Kastner, M. J. Manfra, and D. Goldhaber-Gordon, Clean quantum point contacts in an InAs quantum well grown on a lattice-mismatched InP substrate, *Phys. Rev. B* **105**, 195303 (2022).
- [38] Y. Gul, S. N. Holmes, M. Myronov, S. Kumar, and M. Pepper, Self-organised fractional quantisation in a hole quantum wire, *J. Phys.: Condens. Matter* **30**, 09LT01 (2018).
- [39] L. Liu, Y. Gul, S. N. Holmes, C. Chen, I. Farrer, D. A. Ritchie, and M. Pepper, Possible zero-magnetic field fractional quantization in In<sub>0.75</sub>Ga<sub>0.25</sub>As heterostructures, *Appl. Phys. Lett.* **123**, 183502 (2023).

- [40] S. Kumar, M. Pepper, S. N. Holmes, H. Montagu, Y. Gul, D. A. Ritchie, and I. Farrer, Zero-magnetic field fractional quantum states, *Phys. Rev. Lett.* **122**, 086803 (2019).
- [41] C. Ford, *CryoMeas — A Data-Acquisition Program for LabView* (The University of Cambridge, Cambridge, 2023).
- [42] F. Capotondi, G. Biasiol, I. Vobornik, L. Sorba, F. Giazotto, A. Cavallini, and B. Fraboni, Two-dimensional electron gas formation in undoped  $\text{In}_{0.75}\text{Ga}_{0.25}\text{As}/\text{In}_{0.75}\text{Al}_{0.25}\text{As}$  quantum wells, *J. Vac. Sci. Technol. B* **22**, 702 (2004).
- [43] P. N. Brounkov, T. Benyattou, G. Guillot, and S. A. Clark, Admittance spectroscopy of  $\text{InAlAs}/\text{InGaAs}$  single-quantum-well structure with high concentration of electron traps in  $\text{InAlAs}$  layers, *J. Appl. Phys.* **77**, 240 (1995).
- [44] S. P. Le and T.-K. Suzuki, Electron mobility anisotropy in  $\text{InAs}/\text{GaAs}(001)$  heterostructures, *Appl. Phys. Lett.* **118**, 182101 (2021).
- [45] M. Prager, M. Trottmann, J. Schmidt, L. Ebnet, D. Schuh, and D. Bougeard, Gating of two-dimensional electron systems in  $(\text{In}, \text{Ga})\text{As}/(\text{In}, \text{Al})\text{As}$  heterostructures: The role of intrinsic  $(\text{In}, \text{Al})\text{As}$  deep donor defects, *Phys. Rev. Appl.* **16**, 064028 (2021).
- [46] Y. Gul, G. L. Creeth, D. English, S. N. Holmes, K. J. Thomas, I. Farrer, D. J. Ellis, D. A. Ritchie, and M. Pepper, Conductance quantisation in patterned gate  $\text{In}_{0.75}\text{Ga}_{0.25}\text{As}$  structures up to  $6 \times (2e^2/h)$ , *J. Phys.: Condens. Matter* **31**, 104002 (2019).
- [47] T.-M. Chen, A. C. Graham, M. Pepper, I. Farrer, and D. A. Ritchie, Bias-controlled spin polarization in quantum wires, *Appl. Phys. Lett.* **93**, 032102 (2008).
- [48] G. Shavit and Y. Oreg, Fractional conductance in strongly interacting 1D systems, *Phys. Rev. Lett.* **123**, 036803 (2019).
- [49] F. Capotondi, G. Biasiol, D. Ercolani, and L. Sorba, Scattering mechanisms in undoped  $\text{In}_{0.75}\text{Ga}_{0.25}\text{As}/\text{In}_{0.75}\text{Al}_{0.25}\text{As}$  two-dimensional electron gases, *J. Cryst. Growth* **278**, 538 (2005).
- [50] L. Saminadayar, D. C. Glatthli, Y. Jin, and B. Etienne, Observation of the  $e/3$  fractionally charged Laughlin quasiparticle, *Phys. Rev. Lett.* **79**, 2526 (1997).
- [51] A. Bid, N. Ofek, M. Heiblum, V. Umansky, and D. Mahalu, Shot noise and charge at the  $2/3$  composite fractional quantum Hall state, *Phys. Rev. Lett.* **103**, 236802 (2009).
- [52] R. de Picciotto, M. Reznikov, M. Heiblum, V. Umansky, G. Bunin, and D. Mahalu, Direct observation of a fractional charge, *Nature (London)* **389**, 162 (1997).
- [53] M. Reznikov, R. de Picciotto, T. Griffiths, M. Heiblum, and V. Umansky, Observation of quasiparticles with one-fifth of an electron's charge, *Nature (London)* **399**, 238 (1999).
- [54] M. Dolev, M. Heiblum, V. Umansky, A. Stern, and D. Mahalu, Observation of a quarter of an electron charge at the  $\nu = 5/2$  quantum Hall state, *Nature (London)* **452**, 829 (2008).